IEEE Photonics Journal
An IEEE Photonics Society Publication

Open Access

Generating Chirped Microwave Pulses Using an Integrated Distributed Fabry–Pérot Cavity in Silicon-on-Insulator

Volume 7, Number 2, April 2015

Ming Ma, Student Member, IEEE
Martin Rochette, Senior Member, IEEE
Lawrence R. Chen, Senior Member, IEEE

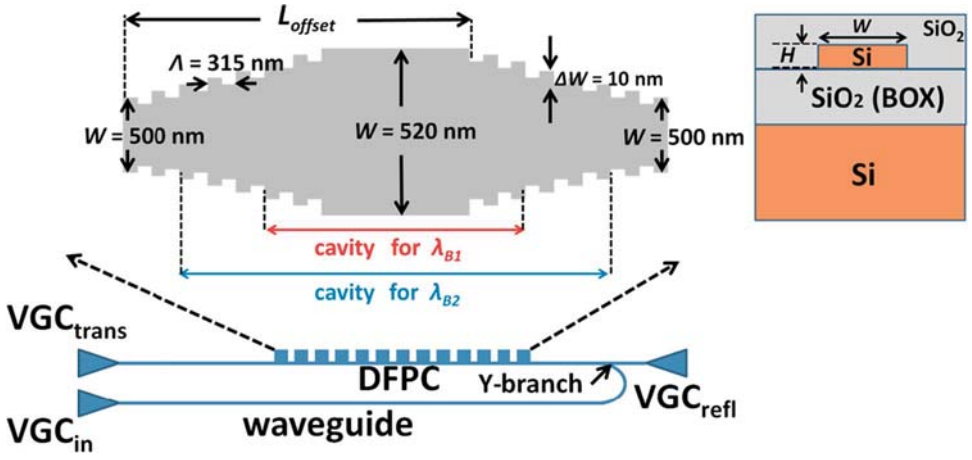

DOI: 10.1109/JPHOT.2015.2417868
1943-0655 © 2015 IEEE

IEEE photonics SOCIETY

IEEE

Generating Chirped Microwave Pulses Using an Integrated Distributed Fabry–Pérot Cavity in Silicon-on-Insulator

Ming Ma, *Student Member, IEEE*, Martin Rochette, *Senior Member, IEEE*, and Lawrence R. Chen, *Senior Member, IEEE*

Department of Electrical and Computer Engineering, McGill University, Montréal, QC H3A 0E9, Canada

DOI: 10.1109/JPHOT.2015.2417868
1943-0655 © 2015 IEEE. Translations and content mining are permitted for academic research only. Personal use is also permitted, but republication/redistribution requires IEEE permission. See http://www.ieee.org/publications_standards/publications/rights/index.html for more information.

Manuscript received March 5, 2015; revised March 25, 2015; accepted March 25, 2015. Date of publication March 30, 2015; date of current version April 10, 2015. This work was supported in part by the Natural Sciences and Engineering Research Council of Canada and in part by the Canadian Microelectronics Corporation. Corresponding author: L. R. Chen (e-mail: lawrence.chen@mcgill.ca).

Abstract: We demonstrate photonic generation of chirped microwave pulses (CMPs) using an integrated distributed Fabry–Pérot cavity (DFPC) in silicon-on-insulator as a spectral shaper. The DPFC is based on a pair of spatially offset chirped Bragg gratings and has a response with varying free spectral range. The spectral shaper is used to filter broadband pulses from a mode-locked fiber laser, and CMPs are obtained at the output of a photodetector following a wavelength-to-time mapping process in a dispersive medium. We generate CMPs with a central frequency of up to 20 GHz, a radio-frequency (RF) chirp of 0.012 GHz/ps, and a time–bandwidth product of 14.5.

Index Terms: Chirped microwave pulse generation, microwave photonics, silicon photonics.

1. Introduction

Chirped microwave pulses (CMPs) have been used widely in various applications, including spread spectrum communications, microwave remote sensing, and microwave computed tomography [1]. While such waveforms can be generated in the electronic domain, their bandwidths, chirp, and central frequencies are limited by the sampling rate of digital electronics. On the other hand, photonic generation of CMPs offers the possibility of achieving central frequencies of tens to hundreds of GHz as well as significant values of chirp, thereby supporting tens of Gigahertz of bandwidth. Indeed, a number of approaches such as direct space-to-time pulse shaping [2], temporal pulse shaping [3], and optical spectral shaping followed by wavelength-to-time mapping [4]–[11] have been used to generate CMPs.

Of the different approaches, optical spectral shaping followed by wavelength-to-time mapping is straightforward to implement. The typical system involves a broadband pulsed source, e.g., a mode-locked fiber laser, a spectral shaper, and a dispersive medium. The spectral shaper modifies the spectrum of the broadband pulses, typically in amplitude only, and the shaped spectrum then propagates through the dispersive medium where a wavelength-to-time mapping process takes place, i.e., the shape of the spectrum is mapped to the time domain. The resulting temporal signal corresponds to the microwave waveform which is detected by a photodetector. The key component in the system is the spectral shaper. It must generate the desired amplitude spectrum

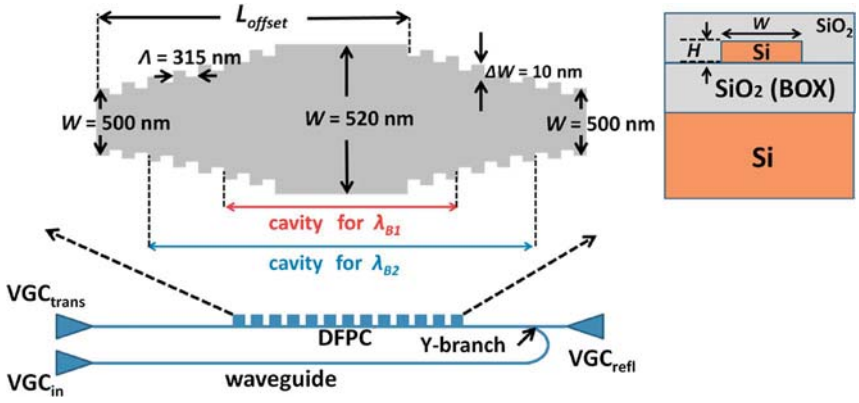

Fig. 1. Schematic (not to scale) of the integrated spectral shaper, along with details of the DFPC and waveguide cross-section.

which ultimately corresponds to the desired microwave waveform. Many different all-fiber spectral shapers have been developed, including a distributed Fabry–Pérot cavity (DFPC) based on spatially offset linearly chirped fiber Bragg gratings (FBGs) [9], a specially designed linearly chirped FBG [10], or a Sagnac loop incorporating a linearly chirped FBG [11].

In the past few years, there has been an increasing emphasis on developing integrated components and subsystems to realize microwave photonic signal processing functions. This has been motivated by the need to address outstanding issues such as compactness, stability, and reliability of so-called "microwave photonic signal processing engines." While integrated microwave photonic devices and subsystems in silicon-on-insulator (SOI), chalcogenide (ChG), and III-V materials have been demonstrated (see [12] for an overview), SOI is of particular interest due to its compatibility with CMOS technology and processing. Recently, Khan *et al.* proposed an integrated spectral shaper based on 8 cascaded microring resonators in SOI [13]. By tuning the resonant wavelengths and coupling strengths of each microring resonator through the use of Mach–Zehnder structures and microheaters, full reconfiguration of the spectral shaper is possible, i.e., at the output port, the wavelengths and amplitudes of the spectral "slices" from each microring can be controlled. Using this integrated device to shape the broadband pulses from a passively mode-locked laser, CMPs with a central frequency of 8 GHz and a radio-frequency (RF) chirp of 0.008 GHz/ps were synthesized. Zhang *et al.* reported an integrated spectral shaper in SOI based on cascading microring resonators in a Mach–Zehnder interferometer [14]. The radii of the microrings differ substantially to provide a large difference in the spectral separation between the microring responses, thereby allowing the generation of CMPs with an RF chirp as large as 0.017 GHz/ps. However, due to the limited number of cascaded microrings, the resulting CMPs comprised only a few cycles (in the time domain), which may restrict their practicality in a number of applications.

In this paper, we present an integrated version of the DFPC in SOI. The Bragg gratings in the integrated DFPC are based on a sidewall corrugations [15] and the chirp is obtained by inducing a linear variation in waveguide width [16]. The integrated DPFC has a spectral response with varying free spectral range (FSR) and we use it to generate CMPs with a central frequency of up to 20 GHz, an RF chirp of 0.012 GHz/ps, and a time–bandwidth product (TBWP) of 14.5. Furthermore, due to the large number of spectral slices in the DFPC response, the corresponding CMPs have a large number of cycles which allows for a reasonable compression ratio of 12.

2. Design of the Integrated DPFC

Fig. 1 shows a schematic of our integrated spectral shaper, along with the cross-section of the device. The Si waveguides have a thickness $H = 220$ nm and width $W = 500$ nm; they sit on top of a 3-μm buried oxide (BOX) layer with a 2-μm-thick index-matched top oxide cladding.

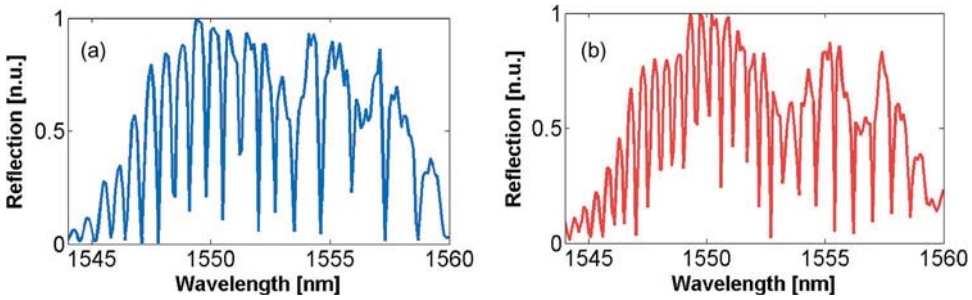

Fig. 2. Spectral response of integrated DFPC with (a) $L_{\text{offset}} = 307.5$ μm and (b) 457.5 μm.

The DFPC comprises two oppositely and linearly chirped Bragg gratings that are separated spatially by a length L_{offset}. The Bragg gratings are based on sidewall corrugations with a depth ΔW; the linear chirp is induced using a linear taper of the waveguide width. The specifications are the following: the nominal grating period is $\Lambda = 315$ nm; the number of periods in each grating is 500, corresponding to a grating length of 157.5 μm; the corrugation depth $\Delta W = 10$ nm; and the waveguide width W varies linearly from 500 nm to 520 nm (or 520 nm to 500 nm) from one end of the grating to the other, giving rise to an estimated grating chirp $C \sim 12.2$ nm/mm.

The wavelength-dependent FSR of the DFPC is [9]

$$\text{FSR}(\lambda) = \frac{\lambda_0^2}{2n_{eff}\left(L_{\text{offset}} - \frac{2}{C}(\lambda - \lambda_0)\right)} \tag{1}$$

where n_{eff} is the effective index of the waveguide, and λ_0 is the starting wavelength. For a fixed grating chirp C, the value of L_{offset} determines the FSR (at a given wavelength). In our experiments, we consider two values of offset—$L_{\text{offset}} = 307.5$ μm and 457.5 μm—to obtain a reasonable number of spectral slices within the bandwidth of interest.

Vertical grating couplers (VGCs) are used to couple light into and out of the integrated spectral shaper and are optimized for TE mode operation. The fiber-to-fiber insertion loss is $\sim$25 dB and each VGC introduces $\sim$10 dB loss. We use the reflection response which is extracted through a Y-branch splitter/combiner. The insertion loss of the DFPC itself is $\sim$5 dB which includes the splitting loss of the Y-branch as well as propagation losses. The total dimensions of the integrated spectral shapers are 720 μm $\times$ 70 μm. The devices are fabricated at the University of Washington Nanofabrication Facility using electron beam lithography with a single full etch.

The spectral responses in reflection are shown in Fig. 2. Clearly, the FSR at a given wavelength is smaller for the integrated spectral shaper having larger L_{offset} and in both cases, the FSR increases with increasing wavelength detuning from λ_0.

3. Experimental Setup and Results

Fig. 3 shows our experimental setup for generating CMPs. A femtosecond mode-locked laser that produces broadband pulses at a repetition rate of 20 MHz is used as the input optical signal. The pulses propagate through $\sim$5 km of single-mode fiber (SMF) before being filtered using the integrated spectral shaper. Erbium-doped fiber amplifiers (EDFAs) are used to compensate for system losses. An optical bandpass filter restricts the operating wavelength range from 1544 nm to 1560 nm and reduces some of the amplified spontaneous emission noise from the EDFAs. Typically, optical spectral shaping is performed first, followed by wavelength-to-time mapping in the dispersive medium; however, the linearity of the system allows for their order to be interchanged without impacting the results (it is also possible to realize both processes simultaneously, as demonstrated in [10]). The generated CMPs are detected using an optical sampling module with 30 GHz bandwidth connected to a communication signal analyzer (CSA) operating in sample mode with a persistence time of 200 ms.

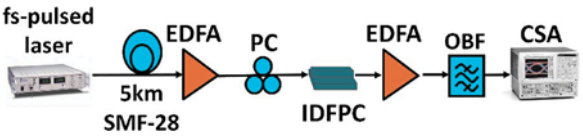

Fig. 3. Experimental setup for generating CMPs based on optical spectral shaping and wavelength-to-time mapping. PC: polarization controller; IDPFC: integrated distributed Fabry–Pérot cavity; OBF: optical bandpass filter.

The instantaneous RF frequency of the CMPs can be approximated by the following expression [9]:

$$f_{RF}(t) \propto 2n_{eff}\left[-\frac{2}{C\lambda_0^2 D^2}t + \frac{2}{C\lambda_0 D} + \frac{L_{\text{offset}}}{\lambda_0^2 D}\right] \tag{2}$$

where D is the dispersion of the dispersive element used for wavelength-to-time mapping. The corresponding RF chirp is

$$\left|\frac{df_{RF}(t)}{dt}\right| = \frac{4n_{eff}}{C\lambda_0^2 D^2}. \tag{3}$$

If we consider a fixed dispersive medium, the RF chirp depends only on the grating chirp C. If further, we consider a given grating chirp C, the spatial offset L_{offset} between the two gratings will determine the central frequency of the CMP at $t = 0$.

The generated CMPs along with the extracted instantaneous frequency vs. time are shown in Fig. 4. The central frequencies and the RF chirps of the CMPs are 15 GHz and 0.011 GHz/ps, and 20 GHz and 0.012 GHz/ps for $L_{\text{offset}} = 307.5$ μm and 457.5 μm, respectively. The measured central frequencies and RF chirps are greater than those predicted by (2) and (3). We attribute these differences due to uncertainty in estimating the grating chirp C and fabrication errors/limitations. First, we estimate the effective chirp in the grating period using the measured reflection response and the simulated values of effective indices. However, this calculation overestimates the actual grating chirp as the reflection bandwidth is typically greater than the simple difference between the Bragg wavelengths at the two ends of the chirped grating [a smaller value of C will increase the instantaneous RF frequency at the pulse center, as well as the RF chirp, per (2) and (3)]. Second, fabrication errors/limitations will cause the fabricated devices to have parameters that differ from the design specifications. However, the measurements verify the general trends that changing L_{offset} will impact the central frequency (the central frequency is higher for the integrated DFPC with a larger L_{offset}) and not the RF chirp (the values are approximately the same in both cases).

The overall duration of the envelopes of the CMPs are $\sim$1100 ps giving rise to estimated TBWPs of 13.3 and 14.5. Fig. 4 also shows the compressed pulses, which are obtained by calculating the autocorrelation traces of the measured CMPs. The full-width half-maximum durations of the compressed pulses are 120 ps and 50 ps for $L_{\text{offset}} = 307.5$ μm and 457.5 μm, respectively, which result in pulse compression ratios of 9 and 12. In principle, the only difference in the CMPs generated by the two integrated DFPCs should be in the central frequencies as the RF chirps and TBWPs should be same. However, variations from fabrication cause differences in the grating chirps and reflection bandwidths and, correspondingly, differences in the RF chirps and TBWPs. Note that the larger pulse compression ratio is obtained using the integrated DFPC with a larger L_{offset} which produces a greater number of spectral slices (and hence, cycles in the time domain waveform [7]).

4. Summary and Conclusion

We have designed and demonstrated an integrated DFPC in SOI for use as a spectral shaper for the photonic generation of CMPs. As a proof-of-concept, we generated CMPs with a central

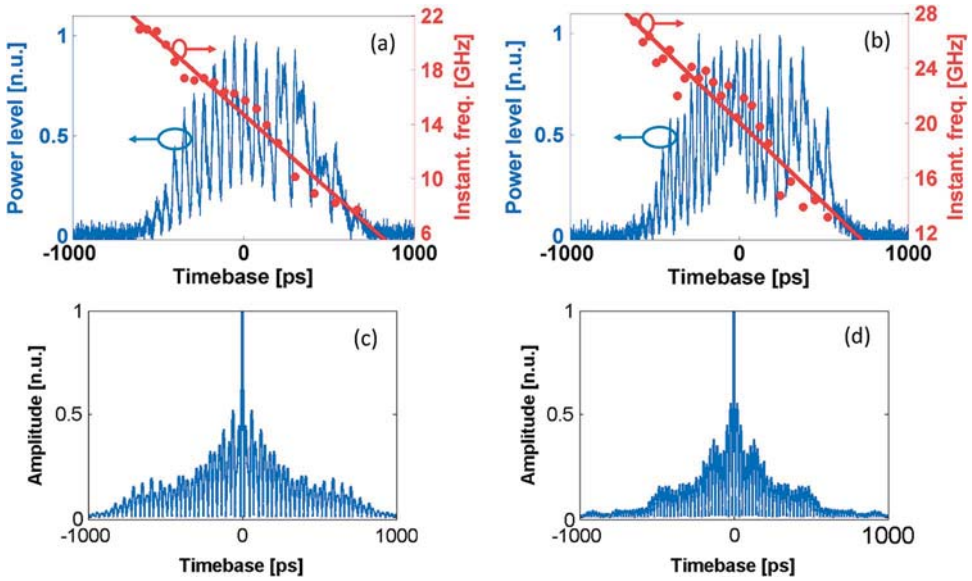

Fig. 4. (a) and (b) Pulse profiles and instantaneous frequency versus time and (c) and (d) calculated auto-correlation showing pulse compression using integrated DFPCs with $L_{\text{offset}} = 307.5\ \mu$m (left) and 457.5 μm (right) for optical spectral shaping.

frequency of 20 (15) GHz, an RF chirp of 0.012 (0.011) GHz/ps, a TBWP of 14.5 (13.3), and a pulse compression ratio of 12 (9). The compression ratio can be enhanced further by increasing L_{offset} to generate more spectral slices (i.e., more cycles in the time domain waveform) and by increasing the TBWP [7]. The TBWP depends on the RF bandwidth and the duration of the envelope of the CMP (denoted ΔT). The RF bandwidth depends on the RF chirp and ΔT, while ΔT depends on the reflection bandwidth of the DFPC and the dispersion D of the medium used for wavelength-to-time mapping. The reflection bandwidth of the DFPC in turn depends on the grating chirp C and length (denoted L_g). Thus, making use of (2), we can show that the TBWP depends only on C and L_g [11]:

$$\text{TBWP} = \left|\frac{df_{RF}}{dt}\right| \Delta T^2 \propto C L_g^2. \tag{4}$$

To increase the TBWP, we can increase the grating chirp and/or length; both can be done readily (within constraints such as a specified dimension/area for the device). However, we must ensure that the reflection bandwidth remains small enough for a linear wavelength-to-time mapping (e.g., to avoid the impact of dispersion slope in the SMF). Generally speaking, these are the same design considerations regardless of whether the DFPC is implemented using FBGs or waveguide gratings.

It may be possible to integrate the entire optical spectral shaping followed by wavelength-to-time mapping system into a single chip by taking advantage of SOI building blocks currently available. For example, chirped Bragg gratings in SOI have been demonstrated that provide several hundred ps of delay over a few nm of bandwidth [16]. Larger values of dispersion, though, are typically required for wavelength-to-time mapping; in this case, some form of loop configuration may be necessary [17]. Large bandwidth germanium photodetectors integrated on SOI waveguide are also available [18], [19] to process CMPs with high central frequencies and large RF chirp. Finally, optical losses need to be reduced further to eliminate the need for optical amplification. To this end, broadband VGCs spanning over 60 nm with a coupling loss as low as 1.74 dB have been realized [20]. By combining our DFPC with the aforementioned building blocks, an integrated system for generating CMPs can be realized in which only a pulsed broadband source is required as the optical input.

Acknowledgment

The devices were fabricated by R. Bojko at the University of Washington Nanofabrication Facility: a member of the National Science Foundation National Nanotechnology Infrastructure Network.

References

[1] A. Rashidinejad and A. M. Weiner, "Photonic radio-frequency arbitrary waveform generation with maximal time–bandwidth product capability," *IEEE/OSA J. Lightw. Technol.*, vol. 32, no. 30, pp. 3383–3393, Oct. 2014.
[2] J. D. McKinney, D. Seo, D. E. Leaird, and A. M. Weiner, "Photonically assisted generation of arbitrary millimeter-wave and microwave electromagnetic waveforms via direct space-to-time optical pulse shaping," *IEEE/OSA J. Lightw. Technol.*, vol. 21, no. 12, pp. 3020–3028, Dec. 2003.
[3] C. Wang, M. Li, and J. Yao, "Continuously tunable photonic microwave frequency multiplication by use of an unbalanced temporal pulse shaping system," *IEEE Photon. Technol. Lett.*, vol. 22, no. 17, pp. 1285–1287, Sep. 2010.
[4] J. Chou, Y. Han, and B. Jalali, "Adaptive RF-photonic arbitrary waveform generator," *IEEE Photon. Technol. Lett.*, vol. 15, no. 4, pp. 581–583, Apr. 2003.
[5] I. Lin, J. D. McKinney, and A. M. Weiner, "Photonic synthesis of broadband microwave arbitrary waveforms applicable to ultra-wideband communication," *IEEE Microw. Wireless Compon. Lett.*, vol. 15, no. 4, pp. 226–228, Apr. 2005.
[6] H. Chi, F. Zeng, and J. Yao, "Photonic generation of microwave signals based on pulse shaping," *IEEE Photon. Technol. Lett.*, vol. 19, no. 9, pp. 668–670, May 2007.
[7] C. Wang and J. Yao, "Photonic generation of chirped millimeter-wave pulses based on nonlinear frequency-to-time mapping in a nonlinear chirped fiber Bragg gratings," *IEEE Trans. Microw. Theory Techn.*, vol. 56, no. 2, pp. 542–553, Feb. 2008.
[8] H. Chi and J. Yao, "Chirped RF pulse generation based on optical spectral shaping and wavelength-to-time mapping using a nonlinearly chirped fiber Bragg grating," *IEEE/OSA J. Lightw. Technol.*, vol. 26, no. 11, pp. 1282–1287, May 2008.
[9] C. Wang and J. Yao, "Photonic generation of chirped microwave pulses using superimposed chirped fiber Bragg gratings," *IEEE Photon. Technol. Lett.*, vol. 20, no. 11, pp. 882–884, Jun. 2008.
[10] C. Wang and J. Yao, "Simultaneous optical spectral shaping and wavelength-to-time mapping for photonic microwave arbitrary waveform generation," *IEEE Photon. Technol. Lett.*, vol. 21, no. 12, pp. 793–795, Jun. 2009.
[11] C. Wang and J. Yao, "Chirped microwave pulse generation based on optical spectral shaping and wavelength-to-time mapping using a Sagnac loop mirror incorporating a chirped fiber Bragg grating," *IEEE/OSA J. Lightw. Technol.*, vol. 27, no. 16, pp. 3336–3341, Aug. 2009.
[12] D. Marpaung *et al.,* "Integrated microwave photonics," *Laser Photon. Rev.*, vol. 7, no. 4, pp. 506–538, Jul. 2013.
[13] M. Khan *et al.,* "Ultrabroad-bandwidth arbitrary radiofrequency waveform generation with a silicon photonic chip-based spectral shaper," *Nat. Photon.*, vol. 4, pp. 117–122, Jan. 2010.
[14] W. Zhang, J. Zhang, and J. Yao, "Largely chirped microwave waveform generation using a silicon-based on-chip optical spectral shaper," in *Proc. Int. Top. Meet. Microw. Photon.*, 2014, pp. 51–53.
[15] X. Wang *et al.,* "Narrow-band waveguide Bragg gratings on SOI wafers with CMOS-compatible fabrication process," *Opt. Exp.*, vol. 20, no. 14, pp. 15 547–15 558, Jul. 2012.
[16] I. Giuntoni *et al.,* "Continuously tunable delay line based on SOI tapered Bragg gratings," *Opt. Exp.*, vol. 20, no. 10, pp. 11 241–11 246, May 2012.
[17] J. Zhang and J. P. Yao, "Time stretched sampling of a fast microwave waveform based on the repetitive use of a linearly chirped fiber Bragg grating in a dispersive loop," *Optica*, vol. 1, no. 2, pp. 64–69, Aug. 2014.
[18] T. Yin *et al.,* "31 GHz Ge n-i-p waveguide photodetectors on silicon-on-insulator substrate," *Opt. Exp.*, vol. 15, no. 21, pp. 13 965–13 971, Oct. 2007.
[19] L. Vivien *et al.,* "42 GHz p.i.n germanium photodetector integrated in a silicon-on-insulator waveguide," *Opt. Exp.*, vol. 17, no. 8, pp. 6252–6257, Apr. 2009.
[20] Y. Ding, H. Ou, and C. Peucheret. "Ultrahigh-efficiency apodized grating coupler using fully etched photonic crystals," *Opt. Lett.*, vol. 38, no. 15, pp. 2732–2734, Aug. 2013.